In vitro reconstitution of Wnt acylation reveals structural determinants of substrate recognition by the acyltransferase human Porcupine

Received for publication, September 6, 2018, and in revised form, October 30, 2018 Published, Papers in Press, November 12, 2018, DOI 10.1074/jbc.RA118.005746

Chul-Jin Lee[‡1], **Mitra S. Rana**[‡], **Chanhyung Bae**[§], **Yan Li**[¶], **and Anirban Banerjee**[‡2]

From the [‡]*Cell Biology and Neurobiology Branch, Eunice Kennedy Shriver National Institute of Child Health and Human Development, National Institutes of Health, Bethesda, Maryland 20892, the* [§]*Molecular Physiology and Biophysics Section, Porter Neuroscience Research Center, NINDS, National Institutes of Health, Bethesda, Maryland 20892, and the* [¶]*Protein/Peptide Sequencing Facility, NINDS, National Institutes of Health, Bethesda, Maryland 20892*

Edited by Karen G. Fleming

Wnt proteins regulate a large number of processes, including cellular growth, differentiation, and tissue homeostasis, through the highly conserved Wnt signaling pathway in metazoans. Porcupine (PORCN) is an endoplasmic reticulum (ER)-resident integral membrane enzyme that catalyzes posttranslational modification of Wnts with palmitoleic acid, an unsaturated lipid. This unique form of lipidation with palmitoleic acid is a vital step in the biogenesis and secretion of Wnt, and PORCN inhibitors are currently in clinical trials for cancer treatment. However, PORCN-mediated Wnt lipidation has not been reconstituted *in vitro* with purified enzyme. Here, we report the first successful purification of human PORCN and confirm, through *in vitro* reconstitution with the purified enzyme, that PORCN is necessary and sufficient for Wnt acylation. By systematically examining a series of substrate variants, we show that PORCN intimately recognizes the local structure of Wnt around the site of acylation. Our *in vitro* assay enabled us to examine the activity of PORCN with a range of fatty acyl-CoAs with varying length and unsaturation. The selectivity of human PORCN across a spectrum of fatty acyl-CoAs suggested that the kink in the unsaturated acyl chain is a key determinant of PORCN-mediated catalysis. Finally, we show that two putative PORCN inhibitors that were discovered with cell-based assays indeed target human PORCN. Together, these results provide discrete, high-resolution biochemical insights into the mechanism of PORCN-mediated Wnt acylation and pave the way for further detailed biochemical and structural studies.

Wnts are secreted signaling proteins that play important roles in asymmetric patterning of embryos and adult tissue homeostasis (1–3). An essential component of biogenesis and secretion of Wnt is post-translational attachment of a specialized lipid, palmitoleic acid, to a highly conserved serine residue by an ER[3]-resident integral membrane enzyme, PORCN (Fig. 1) (4–9). PORCN belongs to the membrane-bound *O*-acyl transferase (MBOAT) family of integral membrane enzymes that catalyze fatty acylation of a diverse spectrum of substrates (10). PORCN is one of the only three known MBOAT family members that work on protein substrates (11). Palmitoleic acid is a monounsaturated fatty acid, making Wnt the only known protein to be modified with such a lipid as well as the only known substrate of PORCN (7, 11). Because Wnt proteins regulate cell proliferation and are misregulated in a number of human cancers, the Wnt signaling pathway has been targeted for development of cancer therapies (1, 12–14). Given the dependence of all of the Wnts, except one, on PORCN for palmitoleoylation and biogenesis, PORCN has been a popular target in the Wnt signaling pathway (15). Progress in medicinal chemistry has led to the discovery of PORCN inhibitors that have shown promise as leads for anticancer drugs (13, 16–18).

Despite the broad importance of the Wnt signaling pathway and PORCN forming an essential component of Wnt biogenesis, it has still not been shown with purified enzyme, *in vitro*, that PORCN is indeed the acyltransferase for Wnt. All of the inhibitor development for PORCN relied on cell-based assays (19, 20); thus, *in vitro* structure–activity relationship studies have not been possible. Although recently Wnt acylation has been reconstituted (21), it used crude membranes rather than purified enzyme. Consequently, it was never conclusively shown that PORCN is necessary and sufficient for acylation of Wnt. Members of the MBOAT family of enzymes have been notoriously recalcitrant to heterologous recombinant purification, and this has been a stumbling block for the field to obtain

This work was supported by National Institutes of Health Grant ZIAHD008928. The authors declare that they have no conflicts of interest with the contents of this article. The content is solely the responsibility of the authors and does not necessarily represent the official views of the National Institutes of Health.

This article contains Figs. S1–S4.

[1] A recipient of the Korean Biomedical Scientist Fellowship Program (KBSFP), supported by the Korean Research Institute of Bioscience and Biotechnology (KRIBB).

[2] To whom correspondence should be addressed. Tel.: 301-496-4855; E-mail: anirban.banerjee@nih.gov.

[3] The abbreviations used are: ER, endoplasmic reticulum; MBOAT, membrane-bound *O*-acyl transferase; TM, transmembrane; αKDH, α-ketoglutarate dehydrogenase complex; PC, 1-palmitoyl-2-oleoyl-*sn*-glycero-3-phosphocholine; PI, 1-palmitoyl-2-oleoyl-*sn*-glycero-3-phosphoinositol; PS, 1-palmitoyl-2-oleoyl-*sn*-glycero-3-phosphatidylserine; POPS, 1-palmitoyl-2-oleoyl-*sn*-glycero-3-phospho-L-serine; ICP-MS, inductively coupled plasma MS; SCD, stearoyl-CoA desaturase; FPP, fluorescence protease protection; eGFP, enhanced GFP; mRFP, monomeric red fluorescent protein; DM, *n*-decyl-β-D-maltoside; RP-HPLC, reversed-phase HPLC; PDB, Protein Data Bank; hPORCN, hWnt1, and hWnt1p, human PORCN, Wnt1, and Wnt1p, respectively.

a refined understanding of their structures, substrate interactions, and mechanisms of action.

Here, we report the first purification and *in vitro* biochemical investigation of Wnt acylation by human PORCN (hPORCN) with purified enzyme preparations. We begin by determining the experimental topology of hPORCN and outline, for the first time in the literature to our knowledge, a method for heterologous overexpression and purification of hPORCN. We demonstrate the enzymatic activity of our purified hPORCN preparation and show that the local structure of Wnt at the site of lipidation is an important determinant for substrate palmitoleoylation by hPORCN. Furthermore, we show that purified hPORCN contains bound zinc ions and demonstrate that it is inhibited by C59 and LGK974, two inhibitors that have been reported in the literature using cell-based assays (13, 17). Finally, because we can control all of the components of our *in vitro* assay, we examine the activity of human PORCN with a range of fatty acyl-CoAs by systematic variation of the fatty acyl chain length and unsaturation. This had not been possible until now because it could not be addressed conclusively whether the selectivity of PORCN for different acyl-CoAs relied on PORCN itself or some other carrier protein that provided the acyl-CoA. Our results show that PORCN likely recognizes the kink in the unsaturated fatty acyl substrate, palmitoleoyl-CoA, and we further dissect its mechanism using mutagenesis to reveal key residues important for its function.

Results

Topological analysis of hPORCN

Several topological models have been put forward for PORCN (22–24). These range from 8 to 11 TM helices that place the C terminus either in the cytoplasm or in the lumen of ER (Fig. 2*B*). We decided to tackle this problem by using selective permeabilization of the plasma membrane and accessibility, to an externally added protease, of a fluorescent protein fused at various parts of hPORCN (Figs. 1*C* and Fig. 2*A*). Briefly, in this cell-based assay, a fluorescent reporter protein is fused at different parts of a transmembrane protein. For an ER-resident integral membrane protein, selective permeabilization of the plasma membrane followed by treatment with a protease only abolishes signal when the fluorescent reporter is exposed to the cytoplasm (25). However, when it faces the lumen of the ER, the fluorescent reporter is protected. In contrast, total permeabilization of all membranes, including organellar membranes, followed by protease treatment abolishes all signals. We systematically evaluated both termini and all of the putative loop regions of hPORCN by this method, and our combined protease accessibility results converged on a 10-TM helix topology model for hPORCN (Fig. 2*C*), thus placing both termini in the cytoplasm. This model is in agreement with model 2 (Fig. 2*B*) proposed by Nile and Hannoush (23). Similar to Hedgehog acyltransferase and ghrelin O acyltransferase, two other MBOAT family members that work on protein substrates, PORCN contains the putative active-site histidine on the ER luminal side. However, a reentrant loop was not found in PORCN, whereas ghrelin *O*-acyltransferase and Hedgehog acyltransferase have one and two putative reentrant loops, respectively (26–28).

Purification and biochemical activity of hPORCN

We evaluated many different parameters for heterologous overexpression and purification of hPORCN. While optimizing this preparation, we paid special attention to using mild detergents so as not to compromise the stability of the purified protein. In addition, modification of the interhelical loop, where significant variation exists among human PORCN isoforms (Fig. S1*A*), enabled us to enhance the stability of the purified hPORCN enzyme. This modified construct (hPORCN_LM) was used for all the *in vitro* biochemical assays (Fig. S1*B*). We also discovered that the addition of the phospholipid 1-palmitoyl-2-oleoyl-*sn*-glycero-3-phospho-L-serine (POPS) was critical to ensuring stability during the purification and monodispersity in size-exclusion chromatographic profile (Fig. S1*C*), leading us to consider POPS as essential for a biochemically well-behaved preparation.

In vitro assay to demonstrate Wnt acylation by hPORCN

The substrate of PORCN is unacylated Wnt. However, purification of Wnt proteins has been mired in considerable technical challenges (29). Moreover, acylation of Wnt is essential for its biogenesis and secretion (30). Thus, even if we were to succeed at isolating and purifying unacylated Wnt, we were uncertain whether it would be properly folded and serve as a substrate. Hence, we decided at the outset to focus on peptide fragments of Wnt as surrogate substrates for demonstrating the activity of PORCN. The structure of XWnt8 bound to the cysteine-rich domain of mouse Frizzled-8 showed that the site of palmitoleoylation has a tongue-shaped structure that is held together by multiple disulfide bonds (5). We speculated that the local structure of this region might be critical in the engagement of PORCN with Wnt and decided to test a substrate representing the sequence of human Wnt1 (hWnt1) from Met-214 to Met-234 with two disulfide bonds (Fig. 3*A*). In an HPLC-based assay, upon incubation with the hPORCN_LM, the peak representing the peptide became lower in intensity, and a new peak appeared that upon mass spectrometric identification was confirmed to be the palmitoleoylated peptide (Fig. 3 (*B* and *C*) and Table 1). Because PORCN is the single enzyme that catalyzes palmitoleoylation of all Wnt proteins, we evaluated sequences corresponding to other Wnts in this assay. Our purified hPORCN_LM preparation also palmitoleoylated substrate fragments corresponding to human Wnt3A (hWnt3A) and human Wnt11 (hWnt11), thus demonstrating that it was able to work on a number of different Wnt sequences as substrates, as would be expected from a functionally active PORCN preparation (Figs. S2 and S3).

To investigate the effect of altering the substrates and the fatty acyl-CoA on the reaction catalyzed by hPORCN, we needed to devise a more high-throughput assay than the HPLC-MS assay described above. We adapted the coupled enzyme assay that has been widely used for assaying DHHC palmitoyltransferases (31–33). This assay (Fig. 4*A*) relies on the free CoA that is released during the acylation reaction from acyl-CoA, and then a second enzyme, α-ketoglutarate dehydro-

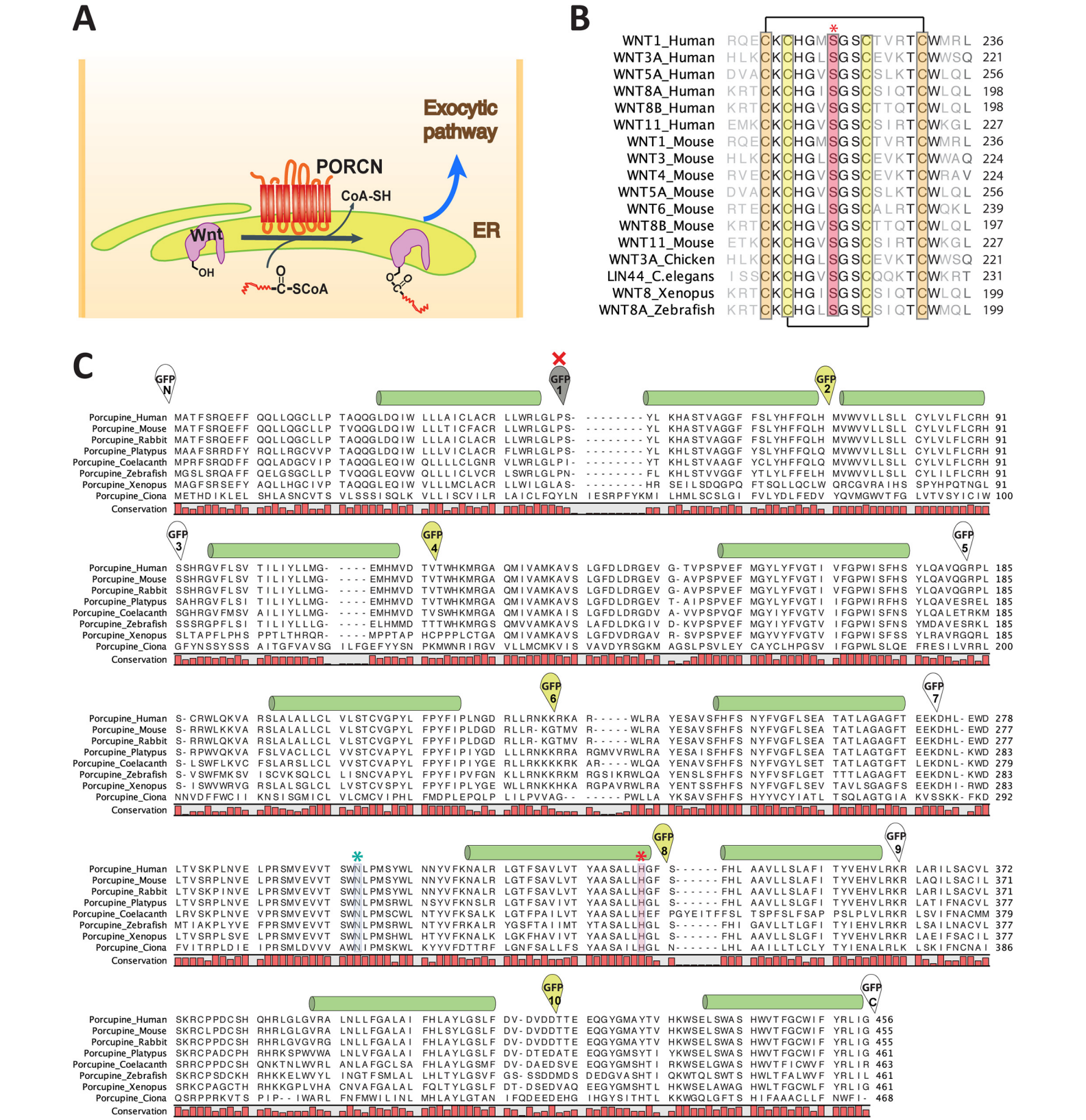

Figure 1. Reaction catalyzed by PORCN and sequence conservation of PORCN and Wnt. *A, schematic* of PORCN-mediated palmitoleoylation of Wnt proteins. PORCN transfers fatty acyl-CoA to a conserved serine residue of Wnt proteins in the ER. *B*, multiple-sequence alignment of the region neighboring the palmitoleoylation site (*asterisk*) of Wnt proteins across different species. Two disulfide bridges formed by two pairs of cysteine residues are indicated. Fully conserved residues are in the *most intense color*. *C*, sequence alignment of PORCN homologs. Predicted transmembrane helices are shown as *cylinders*. Highly conserved asparagine (*blue*) and histidine (*red*) residues are marked by *asterisks*. Positions of GFP insertions for the fluorescence protease protection assay are indicated with *balloons above* the alignment. The GFP/hPORCN fusion constructs with the GFP signals retained or lost after protease treatments are *colored green* or *white*, respectively. The expression of hPORCN-IG1 (*red cross*) was very poor, and thus the data were not interpretable.

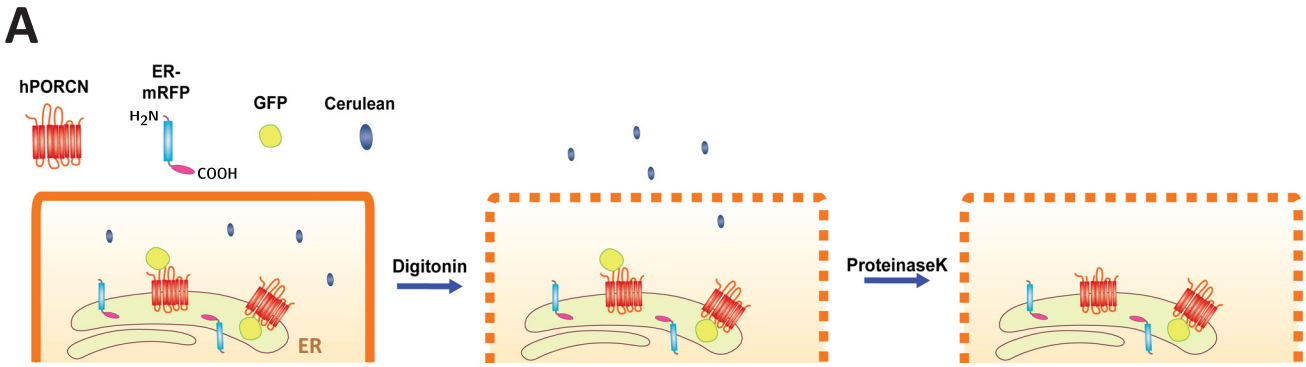

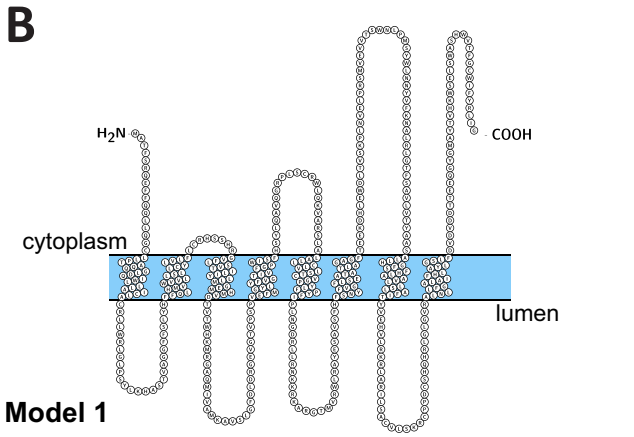

J Biol Chem. 2012 Oct 5; 287(41): 34167-78

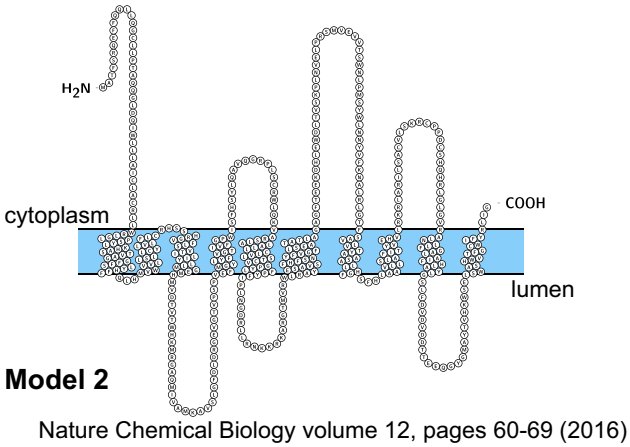

Nature Chemical Biology volume 12, pages 60-69 (2016)

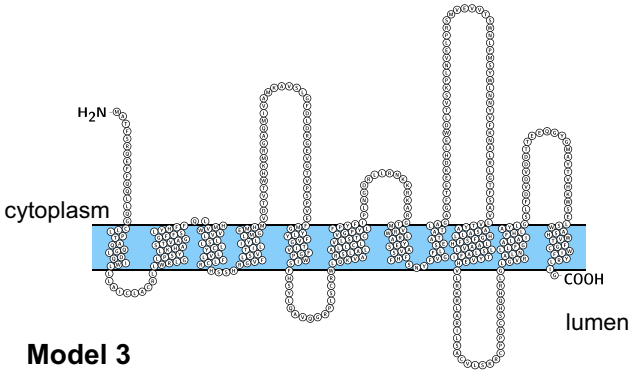

J Biol Chem. 2014 Jun 13;289(24):17009-19

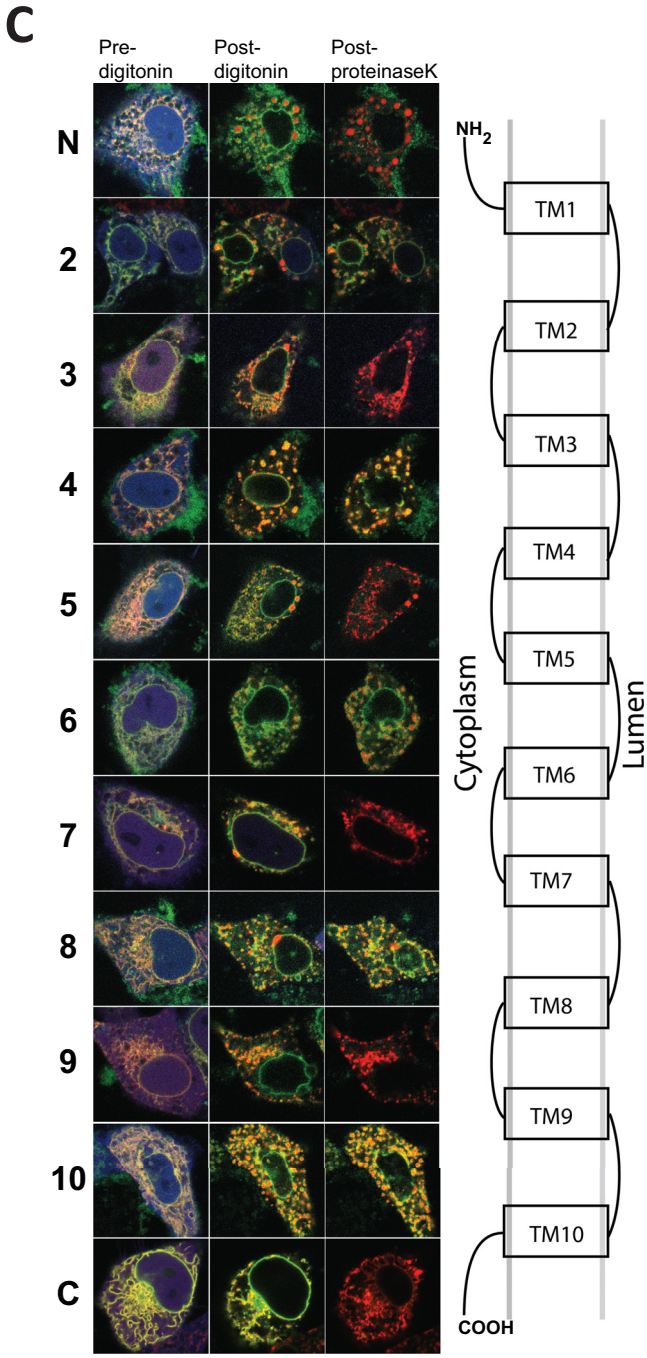

genase complex (αKDH), uses the free CoA to generate succinyl-CoA and NADH. The NADH production can be monitored by fluorescence. Upon incubation with the peptide substrate and palmitoleoyl-CoA in the presence of the components of the coupled enzyme assay, prominent hPORCN activity was detected. In contrast, N301A and H336A mutants of hPORCN, which are thought to be catalytically deficient mutants (4, 22, 24), showed significantly decreased enzymatic activities (Fig. 4*B*). The reaction catalyzed by PORCN bears some similarity to that catalyzed by members of the DHHC family of *S*-acyltransferases that use palmitoyl-CoA to palmitoylate substrate proteins on cysteines. The DHHC members that have been studied *in vitro* have been shown to function by a two-step mechanism where the enzymes undergo autoacylation to form a discrete acyl-enzyme intermediate in the first step (31–33, 37). This first step also results in release of free CoA-SH. In a subsequent step, the autoacylated DHHC enzyme transfers the palmitoyl group to the substrate in a transpalmitoylation reaction. Thus, DHHC enzymes show robust autoacylation activity when treated with palmitoyl-CoA alone in the absence of a protein substrate. We interrogated whether PORCN undergoes a similar autoacylation step by adding all other components of the assay except the peptide substrate. However, we only saw acylation activity from purified hPORCN_LM in the presence of the peptide substrate, suggesting that hPORCN does not form a stable, discrete acylated species. In an effort to further optimize the assay, we tested various lipid additives that could enhance the activity of hPORCN. Of PC, PI, and PS, only PS showed considerable enhancement of hPORCN activity. Hence, all subsequent assays were carried out in the presence of PS (Fig. 4*C*).

Biochemical interrogation of hPORCN

DHHC enzymes contain bound zinc ion that helps in positioning the catalytic residues optimally (31). Because there have been no reports in the literature of homogeneous PORCN preparations, the metal content of PORCN has not been investigated. ICP-MS experiments with our purified hPORCN_LM sample revealed that hPORCN purifies with bound zinc. Measurements with varying concentrations of protein suggested that each protomer of PORCN binds one zinc ion (Fig. 4*E*). To assess the role of the bound zinc in catalytic activity, we attempted to use chelating reagents (EDTA or 4-(2-pyridylazo)resorcinol) to remove the zinc from hPORCN. However, despite trying chelating reagents of various hydrophobicities, we were not able to remove zinc from hPORCN (data not shown).

The enzymatic activity that we observed with the peptide fragment of hWnt1 opened up the possibility of dissecting the molecular basis of interaction between PORCN and Wnt using mutagenesis. Members of the MBOAT family have a highly conserved histidine that is thought to take part in catalysis (10). Mutating this residue in hPORCN to alanine abolished catalytic activity, reinforcing its importance for PORCN function. Measurement of the catalytic activity with varying pH results in a steep increase between pH 6.0 and pH 8.0 with much less variation thereafter, which is consistent with a protonatable histidine involved in catalysis (Fig. 4*D*).

Structural determinants of substrate recognition by hPORCN

To investigate the aspects of the substrate that are important for catalysis by PORCN, we designed a number of substrate variants. However, in doing so, we noted that although there are several known Wnt proteins, there is only one enzyme (*viz.* PORCN) that catalyzes palmitoleoylation of all of them. Thus, to make our conclusions general, we designed the substrate variants based on the sequence, in this region, of a number of different Wnt proteins (Fig. 3*A*). The first panel of substrate fragments that we designed was aimed at investigating the minimal length and the structural constraints necessary for hPORCN to recognize its substrate (Fig. 5*A*). Although hWnt11pC, a substrate corresponding to hWnt11, is efficiently palmitoleoylated, the same substrate without the disulfide bridges shows very little activity, thus underscoring the importance of the disulfide bridges in constraining the local structure of the substrate. In interrogating the minimal length of the substrate recognized by PORCN, hWnt3Ap, with 22 residues and two disulfide bonds, is almost indistinguishable in our assay from hWnt3ApL, with 27 residues and two disulfide bonds. However, both hWnt3ApS, with 8 residues and one disulfide linkage, and hWnt3ApM, with 13 residues and one disulfide linkage, are poor substrates. These data suggest that two disulfide bonds make the minimal unit that is recognized as a substrate by hPORCN. This is reinforced by the fact that hWnt1p_C218A is a poor substrate, whereas hWnt1p, with the same length but two disulfide bonds, is an excellent substrate for hPORCN (Fig. 5*B*). To further investigate the structural requirements imposed by the two individual disulfide bonds, we generated hWnt1p_C220A, a substrate fragment that has the outer disulfide bond, thus possessing the right macrocyclic structure, but no inner disulfide bond, which further constrains the structure of the peptide. Intriguingly, hWnt1p_C220A also proved to be a poor substrate, indicating that the constraints imposed by both of the disulfide bonds are important determinants for substrate recognition by hPORCN.

Besides the highly conserved cysteines that form the disulfide bonded structure, several residues in the surrounding region around the serine, where Wnts become palmitoleoylated, are also highly conserved (Fig. 1*B*). To test whether these are also important for Wnt acylation, we tested several mutants; K309A, H331A, and W323A are all, individually, poor sub-

Figure 2. PORCN topology determination using the fluorescence protease protection assay. *A, schematic* of the FPP assay. HeLa cells expressing mCerulean (*blue oval*), ER-mRFP (*magenta oval*), and hPORCN-GFP (*yellow circle*) fusion proteins were treated with digitonin to permeabilize the plasma membrane, releasing cytosolic mCerulean. Then cells were subjected to the Proteinase K treatment to digest fluorescent tags exposed to the cytosol. *B, graphical representation* of the predicted topologies of PORCN from the literature. *C*, hPORCN tagged with eGFP at the N and C terminus and different loops (Fig. 1*C* and Table 2) are co-expressed with the ER-mRFP and cytosolic mCerulean in HeLa cells. The ER-mRFP protein has fusions of the bovine prolactin signal sequence, mRFP, and a KDEL ER retention sequence, and its red fluorescent tag faces into the ER lumen. Digitonin selectively permeabilizes the plasma membrane. Following digitonin treatment, cells are treated with the protease Proteinase K. A *scheme* of the hPORCN membrane topology consistent with the protease protection results is shown to assist the reader.

A

Indicates a disulfide-bonding cyclization

hWnt1p H_2N - MRQE**C**K**C**HGMSGS**C**TVRT**C**WM -COOH

hWnt1p_C218A H_2N - MRQE**A**K**C**HGMSGS**C**TVRT**S**WM -COOH

hWnt1p_K219A H_2N - MRQE**C**A**C**HGMSGS**C**TVRT**C**WM -COOH

hWnt1p_C220A H_2N - MRQE**C**K**A**HGMSGS**S**TVRT**C**WM -COOH

hWnt1p_H221A H_2N - MRQE**C**K**C**A**G**MSGS**C**TVRT**C**WM -COOH

hWnt1p_S224T H_2N - MRQE**C**K**C**HGM**T**GS**C**TVRT**C**WM -COOH

hWnt1p_W234A H_2N - MRQE**C**K**C**HGMSGS**C**TVRT**C**A**M** -COOH

hWnt1pL H_2N - SEMRQE**C**K**C**HGMSGS**C**TVRT**C**WMRLPT -$CONH_2$

hWnt3ApS H_2N -**C**HGLSGS**C**-COOH

hWnt3ApM H_2N -K**C**HGLSGS**C**EVKT-COOH

hWnt3Ap H_2N - MHLK**C**K**C**HGLSGS**C**EVKT**C**WWS -COOH

hWnt3ApL H_2N - ASMHLK**C**K**C**HGLSGS**C**EVKT**C**WWSQPD -$CONH_2$

hWnt8BpM H_2N -K**C**HGVSGS**C**TTQT-COOH

hWnt11pO H_2N -LEMK**C**K**C**HGVSGS**C**SIRT**C**WKGL-COOH

hWnt11pC H_2N -LEMK**C**K**C**HGVSGS**C**SIRT**C**WKGL-$CONH_2$

B

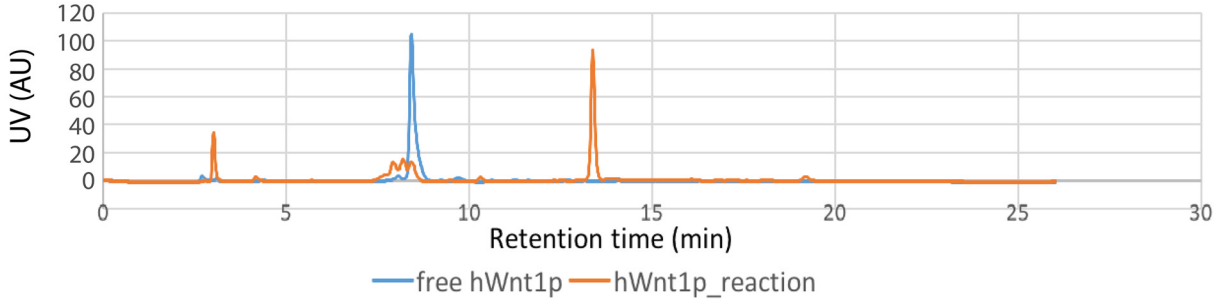

C

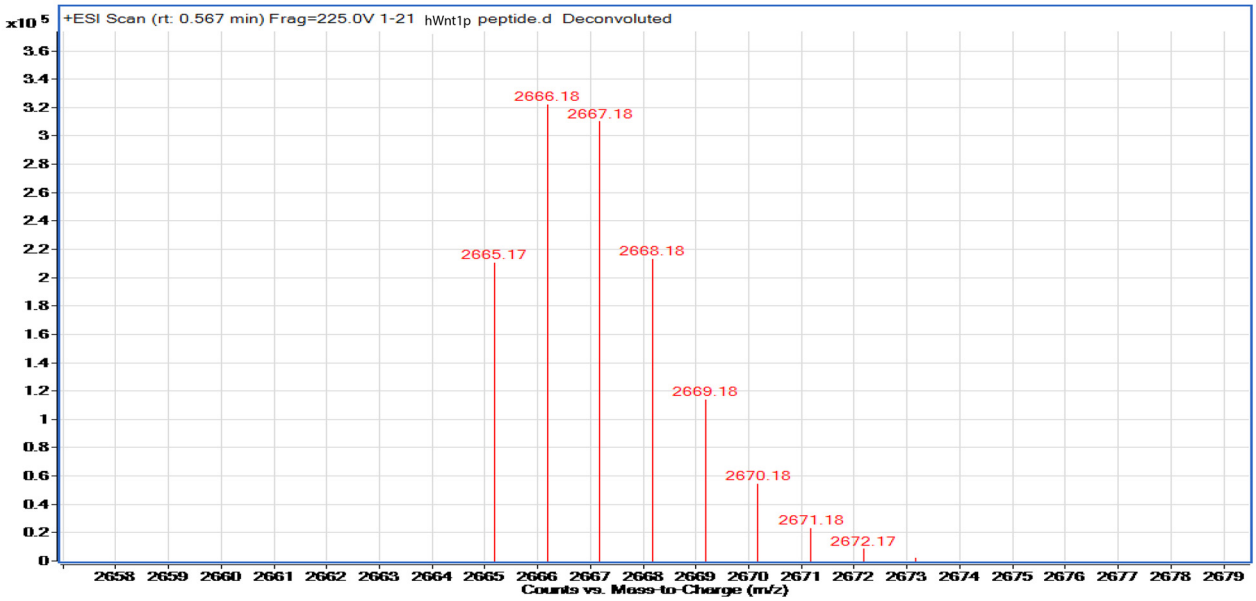

Table 1
Monoisotopic mass of free or palmitoleoylated peptides

	Free form		Palmiltoleoylated form	
$[M + H]^+$	Monoisotopic mass calculated	Monoisotopic mass measured	Monoisotopic mass calculated	Monoisotopic mass measured
hWnt1p	2428.98	2428.95	2665.19	2665.17
hWnt3Ap	2518.11	2518.10	2754.32	2754.31
hWnt11pC	2520.18	2520.20	2756.39	2756.37
hWnt1pL	3111.34	3111.34	3347.55	3347.53
hWnt3ApL	3015.32	3015.32	3251.53	3251.51

strates for Wnt, arguing for these residues to be important aspects of Wnt–PORCN interaction (Fig. 5*B*).

PORCN inhibitors

Owing to the importance of Wnt proteins in cellular proliferation, differentiation, migration, and polarity, inhibitors of Wnt signaling pathway have recently attracted attention as therapeutic avenues for Wnt-driven cancers. Because the palmitoleoylation by PORCN is essential for the biogenesis and secretion of Wnt, PORCN is a prominent target for developing such inhibitors for various cancers. Several hPORCN inhibitors have been reported in the literature. However, these compounds were discovered through cell-based assays, and their action on hPORCN has never directly been demonstrated through an *in vitro* assay with purified enzyme. We decided to focus on two of these inhibitors, LGK-974 and C59 (13, 17). LGK-974 is currently in clinical trials. In ITC experiments, LGK-974 bound to purified hPORCN_LM with a K_d of 0.39 μM (Fig. 5*C*). C59 is particularly insoluble in aqueous buffers, making its ITC experiment particularly challenging. Thus, the inhibition of hPORCN by C59 was tested using the coupled enzyme assay, resulting in an IC_{50} of 0.67 μM (Fig. 5*D*). Although LGK-974 was comparatively more soluble, the compound is fluorescent, thus interfering with the signal from NADH in the coupled enzyme assay. Hence, the IC_{50} of LGK-974 was not determined.

Fatty acyl-CoA selectivity

PORCN uses a noncanonical fatty acyl-CoA (*i.e.* palmitoleoyl-CoA with an unsaturation in the middle of the fatty acyl chain). This causes a prominent kink in the ground state conformation of the fatty acyl chain. However, there is currently no understanding about the shape of the binding site where PORCN binds palmitoleoyl-CoA. It is also not known how the activity of PORCN depends on the length of the fatty acyl chain and the specific position of the unsaturation. To investigate the fine-grained constraints in the fatty acyl chain recognition by PORCN, we systematically evaluated a series of fatty acyl-CoAs as shown in Fig. 6*A*. Because our assay is assembled completely *in vitro*, we could control all of the components and examine the preference of PORCN for other CoAs, keeping everything else identical. Interestingly, among the saturated acyl-CoAs, there is an increase in the catalytic activity from hexanoyl-CoA ($n = 6$) to decanoyl-CoA ($n = 10$), after which there is an abrupt drop for dodecanoyl-CoA ($n = 12$). Upon further increase in the fatty acyl chain length, the activity stays at approximately the same level until the unsaturated palmitoleoyl-CoA, which is the best substrate for hPORCN. Interestingly, there is a very sharp drop in catalytic activity when we tested unsaturated fatty acyl-CoAs with more carbon atoms than palmitoleoyl-CoA, thus indicating that these are poor substrates. These data indicate that PORCN recognizes both the position of the kink in the acyl chain and the length of the fatty acyl chain.

Discussion

More than 10 years after the discovery that secreted Wnt proteins have a monounsaturated fatty acyl modification that is indispensable for the biogenesis and function of Wnt proteins, there has been very little biochemical characterization of PORCN, the enzyme responsible for catalyzing this modification. The reason for this gap of knowledge is that that there has been no report of successful purification of PORCN from native or heterologous sources. Here, we have successfully overexpressed and purified human PORCN and have demonstrated its catalytic activity through a reconstituted *in vitro* assay with fragments of a number of Wnt proteins. This part of Wnt is held together by two disulfide bonds. Although it has been shown that a peptide fragment can act as a surrogate substrate for PORCN (21), the structural constraints that are needed were not probed. Our studies reveal the detailed local structural constraints on Wnt that enable it to be utilized as a substrate of PORCN and show that a linear substrate or one with a single disulfide bond is a poor substrate, whereas one with two disulfides is a much better substrate. These results indicate that the local structure around the site of acylation is an important feature in the recognition of Wnt substrates by PORCN. This suggests that PORCN makes contacts with several residues in this region and is able to "read out" the fine structural details of the substrate. This is consistent with the high degree of sequence conservation in Wnt proteins in this specific region. Furthermore, we have experimentally determined the topology of hPORCN, demonstrating that hPORCN has 10 TM helices with both the N and the C termini in the cytosol.

The fact that PORCN does not have an obviously recognizable zinc-binding motif in any of its extramembranous segments leads to the possibility that the transmembrane domain harbors part of the zinc-binding site and that the bound zinc ion takes active part in catalysis. The binding of zinc ion is reminiscent of functionally related DHHC enzymes that catalyze fatty acylation of proteins with saturated fatty acids, predominantly

Figure 3. LC-MS analysis of PORCN mediated Wnt fatty acylation using the Wnt fragments. *A*, hWnt1pL, hWnt3ApL, and hWnt11pC have been synthesized with a C-terminal amide. *B*, reverse-phase HPLC chromatogram of free hWnt1p and palmitoleoylated hWnt1p**.** *C*, *zoomed-in* mass range for the $[M + H]^+$ ions of the palmitoleoylated hWnt1p sample.

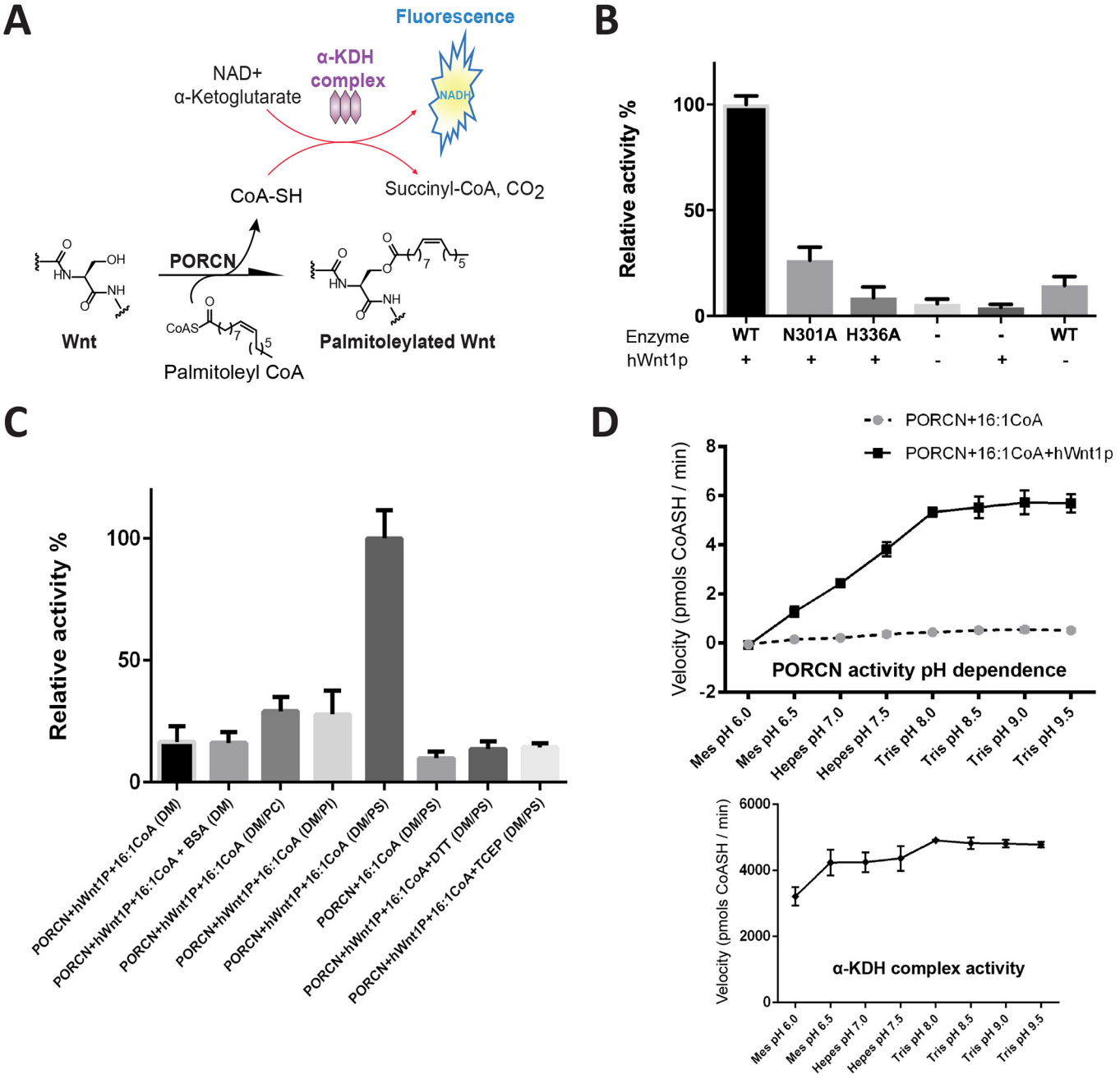

sample	Measured protein conc. (μM)	ICP-MS Zn conc. (μM)	Ratio (Zn/protein)
Buffer	0	0.379	ND
12 μM	12	11.8	0.98
24 μM	24	26.7	1.11
32 μM	32	37.1	1.16

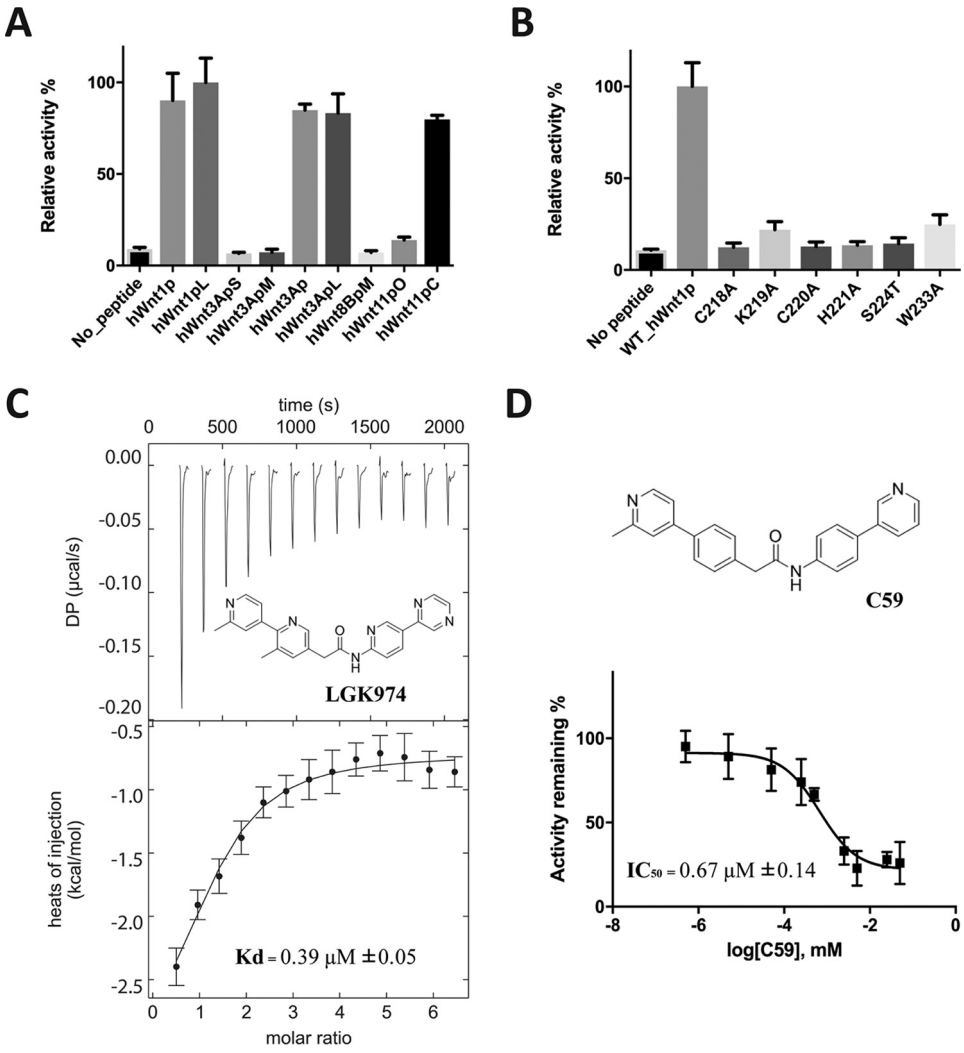

Figure 5. Structural and mutational dissection of Wnt using the coupled enzyme assay and biochemical characterization of hPORCN inhibition. *A*, graphs represent PAT activities using the synthetic Wnt peptides varied in length, sequence, and the number of disulfide bonds. Purified hPORCN (500 nM) was incubated with 50 μM Wnt peptides in the presence of 50 μM palmitoleoyl-CoA. The sequences of the peptides are shown in Fig. 3*A*. *B*, the hPORCN was incubated with 50 μM of WT hWnt1p peptide (*hWnt1P*) or hWnt1p mutants in the presence of 50 μM palmitoleoyl-CoA. *C*, isothermal titration calorimetric titration of LGK974 binding to purified hPORCN. *D*, IC_{50} curve for hPORCN inhibition by C59. IC_{50} values were determined by fitting a three-parameter dose–response curve (GraphPad Prism); $n = 3$; *error bars*, S.D.

palmitic acid, at the cytosolic face of the membrane. In the case of DHHC enzymes, although they bind two zinc ions per monomer, the zinc ions play a structural role rather than taking an active part in catalysis (31). Further experiments will delineate the specific functional role of zinc ions for PORCN. Unlike DHHC enzymes, however, hPORCN does not form a stable autoacylated enzyme that we can detect in our assays. This suggests that binding of the substrate Wnt triggers a conformational rearrangement that drives the catalytic reaction forward.

One critical question about PORCN is its selectivity for acyl-CoAs of different chain length and shape. The critical structural aspect of palmitoleoyl-CoA that is different from the saturated fatty acyl CoA is the distinct bend in the acyl chain that is formed by the *cis* double bond in its lowest-energy conformation. Existing structures reveal that proteins that are involved in the biosynthesis of palmitoleoyl-CoA (*i.e.* stearoyl-CoA desaturase (SCD)) (34, 35) or proteins that specifically recognize the unsaturated aliphatic chain (*i.e.* Wnt deacylase Notum) (36) assert selectivity for the unsaturated fatty acyl group by forming a bent acyl-chain– binding cavity in which the shape of the cavity closely mimics this bent conformation of the palmitoleoyl chain (Fig. 6*C*). To interrogate whether PORCN has a similar cavity, we tested the fatty acyl selectivity of hPORCN, and intriguingly, the selectivity for saturated acyl-CoAs drops

Figure 4. Coupled enzyme assay for hPORCN acylation activity. *A*, schematic of the coupled-enzyme assay. *B*, purified WT and N301A and H336A mutants of PORCN (500 nM) were incubated with 50 μM of hWnt1p peptide and 50 μM palmitoleoyl-CoA. Activity was normalized to WT PORCN (100%). *Graphs* represent the relative protein acyltransferase (*PAT*) activities of WT, N301A, and H336A, along with the reaction without adding the peptide, the reaction with only palmitoleoyl-CoA, and the reaction with only palmitoleoyl-CoA and the peptide. *C*, PAT activities in the presence of different additives. Percentage activity was normalized to that in the presence of POPS. *D*, hPORCN activity is shown as a function of pH as well as that of αKDH complex in the *bottom panel*. The coupled reaction rate is dominantly fast enough not to limit the palmitoleoylation reaction. The assay conditions for *C* and *D* were the same as for *B*. *E*, ICP-MS analysis of purified hPORCN sample. The *table* (*inset*) shows the zinc/protein ratios for the different measurements. $n = 3$; *error bars*, S.D.

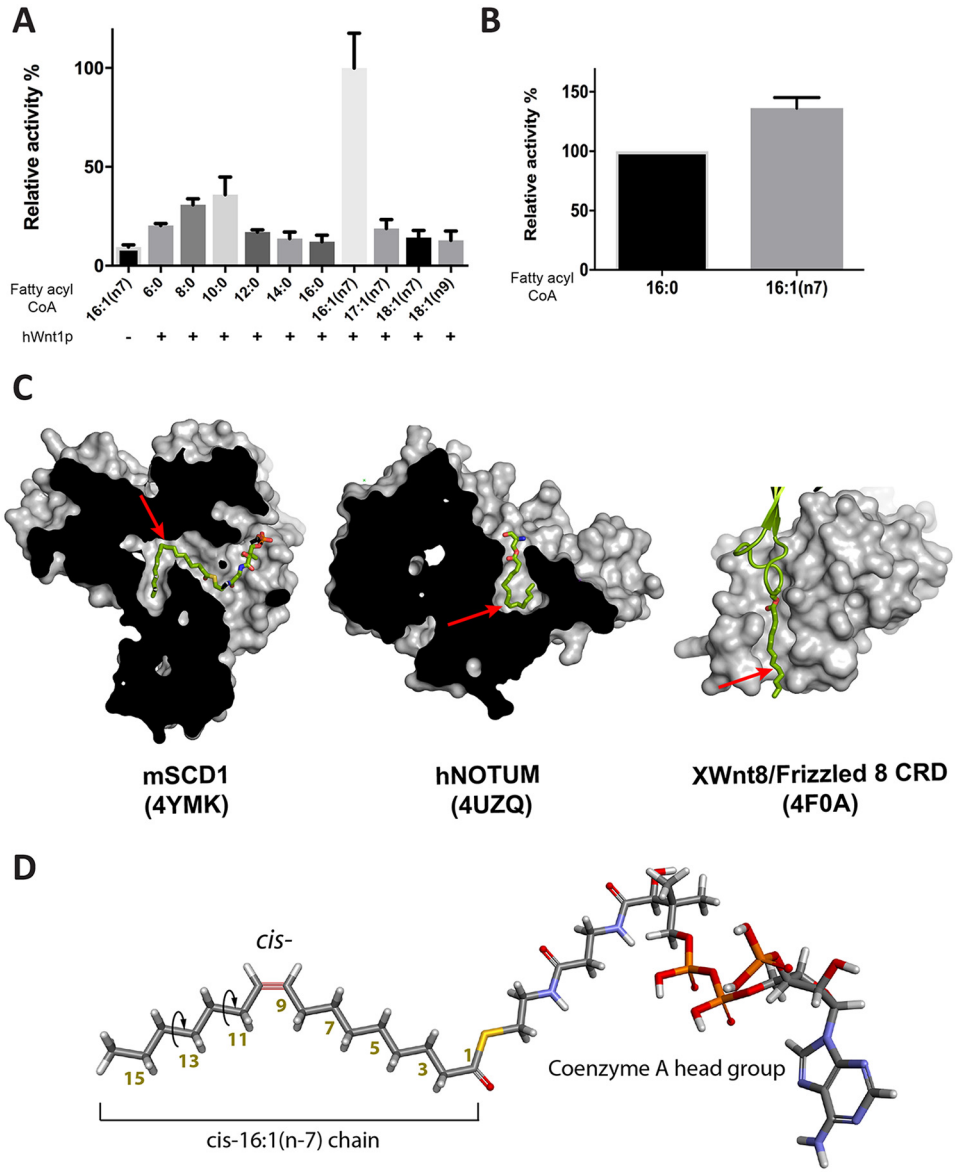

Figure 6. Fatty-acyl-CoA selectivity of PORCN. *A*, graph showing hPORCN activity for acyl-CoAs of varying saturated hydrocarbon chain lengths (C6:0–C16:0) and unsaturated lengths (palmitoleoyl-CoA; C16:1(*n*-7)), heptadecenoyl-CoA (C17:1(*n*-7)), *cis*-vaccenoyl-CoA (C18:1(*n*-7)), and oleoyl-CoA (C18:1(*n*-9)). *B*, fatty acyl-CoA selectivity assay for human DHHC20 palmitoyltransferase measured with a coupled-enzyme assay. Selectivity is normalized to palmitoyl-CoA (16:0 CoA). Data are the average ± S.E. (*error bars*) from three independent measurements. *C*, molecular rendition (*gray*) of mSCD1 (PDB code 4YMK), hNOTUM (PDB code 4UZQ), and XWnt8 in complex with Frizzled 8 CRD (PDB code 4F0A). The bound fatty-acid chains are *highlighted* in *green*. *Arrowheads*, positions of the double bonds within the acyl chains. *D*, a *stick model* of unsaturated (*cis*-C16:1(*n*-7)) palmitoleoyl-CoA, showing the kink around the *cis* double bond of the acyl group. The *round arrows* indicate rotations around carbon–carbon single bonds that can result in a more linear structure.

sharply after C10. Considering that the unsaturation in palmitoleoyl-CoA is right in the middle of the acyl chain, this prediction closely agrees with where the kink in the acyl chain of palmitoleoyl-CoA occurs. In other words, in a bent cavity mimicking the shape of the palmitoleoyl chain, the length of the C10 acyl chain would roughly correspond to the first arm of the cavity (Fig. 6*D*). hPORCN also sharply discriminates between C16:0, the saturated palmitoyl-CoA, and its cognate substrate, C16:1, palmitoleoyl-CoA. All of these data suggest that hPORCN has a bent cavity where the palmitoleoyl-CoA binds (23). Notably, hPORCN also is highly selective for C16:1 over C18:1. This indicates that the length of the second arm of the cavity of hPORCN is a snug fit for palmitoleoyl-CoA and does not allow for promiscuity with regard to the acyl chain length. It is important to note here that the enzyme that generates the monounsaturated acyl-CoAs, SCD, resides in the same ER membrane as PORCN. SCD generates both C18:1 and C16:1 CoA. However, Wnts are predominantly modified with C16:1. Our results show how this selective screening occurs at the stage of PORCN.

Interestingly, the structure of XWnt8 bound to the cysteine-rich domain of mouse Frizzled-8 reveals the acyl group in XWnt8 binding in a more linear conformation to the extracellular domain of Frizzled-8 (5). This is in sharp contrast to the bent acyl chains binding to the hydrophobic cavities seen in the structures of SCD or Notum (34–36). Although the authors were not able to verify whether or not the acyl chain in their preparation was an unsaturated palmitoleoyl group, this sug-

Table 2
GFP/hPORCN fusion constructs used for the fluorescence protease protection assay
Downward arrows indicate the GFP insertion sites of the fusion constructs.

	Location of eGFP inserted to human PORCN encoded	Linker at the N terminus of eGFP	Linker at the C terminus of eGFP
hPORCN-NG	↓ M^{1}		(eGFP)-LEVLFQGPSRAGGSGGSGGSGT-M^{1}
hPORCN-CG	G^{456} ↓	G^{456}-SNSLEVLFQGPTAAGGSGG SGGSGAAVSK-(eGFP)	
hPORCN-IG1	P^{48} ↓ S^{49}	P^{48}-GPTAGGSGGSGGSGAAA-(eGFP)	(eGFP)-SGGSAGGSATGGSGHS-S^{49}
hPORCN-IG2	H^{71} ↓ M^{72}	H^{71}-GPTAGGSGGSGGSGAAA-(eGFP)	(eGFP)-SGGSAGGSATGGSGHS-M^{72}
hPORCN-IG3	S^{92} ↓ S^{93}	S^{92}-GPTAGGSGGSGGSGAAA-(eGFP)	(eGFP)-SGGSAGGSATGGSGHS-S^{93}
hPORCN-IG4	V^{118} ↓ T^{119}	V^{118}-GPTAGGSGGSGGSGAAA-(eGFP)	(eGFP)-SGGSAGGSATGGSGHS-T^{119}
hPORCN-IG5	G^{182} ↓ R^{183}	G^{182}-GPTAGGSGGSGGSGAAA-(eGFP)	(eGFP)-SGGSAGGSATGGSGHS-R^{183}
hPORCN-IG6	K^{231} ↓ R^{232}	K^{231}-GPTAGGSGGSGGSGAAA-(eGFP)	(eGFP)-SGGSAGGSATGGSGHS-R^{232}
hPORCN-IG7	K^{272} ↓ D^{273}	K^{272}-GPTAGGSGGSGGSGAAA-(eGFP)	(eGFP)-SGGSAGGSATGGSGHS-D^{273}
hPORCN-IG8	F^{338} ↓ S^{339}	F^{338}-GPTAGGSGGSGGSGAAA-(eGFP)	(eGFP)-SGGSAGGSATGGSGHS-S^{339}
hPORCN-IG9	K^{361} ↓ R^{362}	K^{361}-GPTAGGSGGSGGSGAAA-(eGFP)	(eGFP)-SGGSAGGSATGGSGHS-R^{362}
hPORCN-IG10	D^{418} ↓ T^{419}	D^{418}-GPTAGGSGGSGGSGAAA-(eGFP)	(eGFP)-SGGSAGGSATGGSGHS-T^{419}

gests two aspects about the recognition of the fatty acyl chain by Frizzled. 1) Frizzled receptors do not have the same shape selective cavity for a palmitoleic acid lipid group like SCD or Notum, which begs speculation that the unsaturated fatty acyl group is only required at the earlier stages of the Wnt signaling pathway. 2) Assuming that the acyl chain in the XWnt8–Frizzled complex is indeed a palmitoleoyl group, it can nevertheless adopt a more linear-like conformation by rotation about the carbon–carbon single bonds. The associated energetic cost is likely compensated by favorable interactions with the acyl chain–binding groove in Frizzled (5) (Fig. 6, *C* and *D*).

Another intriguing aspect of the fatty acyl selectivity of hPORCN is a comparison of its selectivity between C16:0 and C16:1 with that of members of the DHHC family of enzymes. DHHC enzymes catalyze acylation of their substrates in two steps. The first step is an autoacylation of the enzyme that also reflects the fatty acyl chain selectivity of the enzyme (37). In a coupled enzyme assay, human DHHC20 shows very little selectivity for C16:0 over C16:1 (Fig. 6*B*). We recently solved the crystal structure of human DHHC20 and zebrafish DHHC15 (31). Both structures show that DHHC enzymes form a cavity in the membrane where the acyl chain binds. Presumably, this cavity can accommodate both a saturated acyl chain and an unsaturated acyl chain, most likely in a similar linear-like conformation. Our data suggest that the cavity in hPORCN is considerably more constrained, thus creating a large penalty for accommodating the saturated acyl-CoA.

Experimental procedures

Plasmid construction and molecular biology

Synthetic human PORCN codon-optimized DNA (DNA 2.0) was cloned into a pPICZ-C vector for *Pichia pastoris* expression with a PreScission cleavage site followed by an eGFP coding sequence and a 10× His tag at the C terminus. To generate a construct for expressing more stable human PORCN protein, 14 amino acids (PYFIPLNGDRLLRN, residues 216–229) in an interhelical loop were removed, and mutations for C187A (a potential palmitoylation site) (4), A194S, K231G, R232T, K233M, and A234V were performed by Phusion site-directed mutagenesis. Sequence alignment between WT human PORCN and the modified version is shown in Fig. S1*B*. The vector containing the modified human PORCN sequence was used as a cloning template of single point mutations for human PORCN mutant analyses.

WT human *PORCN* gene obtained from Open Biosystems (GE Lifesciences) was cloned into a pEGFP vector (Addgene) with a cytomegalovirus promoter for expression in HEK293T cells. For a fluorescence protease protection (FPP) assay, an eGFP coding sequence was inserted at the N terminus, C terminus, or interhelical loops of human PORCN by exponential megapriming PCR (38) or Gibson assembly (39) cloning methods. For protease accessibility to the eGFP fusion tag, a linker region was inserted between the eGFP and human PORCN sequences using the site-directed mutagenesis. Constructs used for the FPP assay are listed in Table 2.

Fluorescence protease protection assay

The fluorescence protease protection assay was performed essentially as described previously (25). HeLa cell cultures were maintained in Dulbecco's modified Eagle's medium supplemented with fetal bovine serum, glutamine, and penicillin/streptomycin in a humidified incubator at 37 °C with 5% CO_2. HeLa cells were seeded onto 8-well glass-bottom imaging chambers (Nunc LabTek II) in the evening prior to the day of transfection. The next day, cells in each well were transiently transfected with 150 ng of DNA of hPORCN constructs along with 75 ng of mCerulean and 75 ng of ER-mRFP (25, 40) using Lipofectamine 3000 (Invitrogen) according to the manufacturer's instructions. 48 h after transfection, cells were washed with KHMC buffer (110 mM potassium acetate, 20 mM HEPES-NaOH, pH 7.2, 3 mM magnesium chloride, and 10 mM calcium chloride) and then maintained in 250 μl of the same. 40 μM digitonin (Calbiochem) and 0.6 mg/ml Proteinase K (Worthington) solutions were freshly prepared in KHMC buffer.

To permeabilize the plasma membrane, 250 μl of 40 μM digitonin was added to the cells in the wells to give a final digitonin concentration of 20 μM. Progress was followed by time-lapse imaging with an interval of 2 min to prevent photobleaching. Once the cytoplasmic mCerulean signal disappeared, indicating plasma membrane permeabilization, imaging was stopped. The time interval was then changed to 15 s, and imaging was restarted followed by the addition of 100 μl of Proteinase K solution to give a final protease concentration of ~100–120 μg/ml. Imaging after protease addition was carried out for 2.5–3.5 min (10–15 cycles). All imaging was done on a Zeiss LSM780 confocal microscope with a Plan-Apochromat ×63/1.40 numerical aperture oil objective. Images were processed and created using the freely available software FIJI (41).

Yeast transformation, protein expression, and purification

The pPICZ vectors containing the human PORCN expression constructs were electroporated into *P. pastoris* strain SDM1163, and the transformants were plated on YPDS plates containing 700 μg/ml Zeocin (Invitrogen). Protein expression by selected colonies in 1–2-ml scale cultures were assessed using fluorescence-detection size-exclusion chromatography (42). For large-scale purification, selected colonies were grown in 20 ml of YPD medium overnight at 30 °C. These overnight cultures were then used to inoculate 1.5-liter BMGY (0.1 M potassium phosphate, pH 6.0, 3.4 g/liter yeast nitrogen base, 1% glycerol, 0.4 μg/ml biotin, 100 μg/ml Zeocin) cultures. Cells were allowed to grow for ~24 h to an A_{600} of ~20 at 30 °C. Then cells were pelleted by centrifugation and resuspended in 1.5 liters of BMMY (0.1 M potassium phosphate, pH 6.0, 3.4 g/liter yeast nitrogen base, 1% methanol, 0.4 μg/ml biotin, 25 μg/ml Zeocin). Cells were incubated for another ~36 h at 23 °C. Cells were harvested by centrifugation. The pelleted cells were flash-frozen in liquid nitrogen and stored at −80 °C. Frozen cells were disrupted using Retsch MM400 millers with liquid nitrogen cooling. ~26 g of milled cell powder was suspended in ~200 ml of lysis buffer containing 100 mM HEPES, pH 7.9, 450 mM NaCl, 1 mM tris(2-carboxyethyl)phosphine, 1.5% (w/v) *n*-dodecyl-β-D-maltoside, 0.1% (w/v) cholesteryl hemisuccinate, protease inhibitors (benzamidine, 4-(2-aminoethyl)-benzenesulfonyl fluoride hydrochloride, soy trypsin inhibitor, pepstatin, leupeptin), and DNase. The lysate was extracted using a magnetic stirrer at 4 °C for 1 h and then centrifuged at 38,000 × *g* for 30 min at 4 °C. The supernatant was loaded onto a column containing 3 ml of TALON resin (Clontech). The column was washed with 2.5 column volumes of wash buffer containing 25 mM Tris-HCl, pH 7.8, 350 mM NaCl, 1 mM tris(2-carboxyethyl)phosphine, 4 mM *n*-decyl-β-D-maltoside (DM), 20 mM imidazole, and 0.1 mg/ml POPS (obtained from Avanti) followed by an additional wash with 1.5 column volumes of the same buffer without imidazole. Prior to on-column PreScission protease cleavage, the protein-bound resin was resuspended in 2 column volumes of wash buffer without imidazole. The resin slurry was then rotated for 5 h at 4 °C. The cleaved protein was collected by gravity flow and concentrated with a 50,000 molecular weight cut-off 15-ml concentrator (Millipore) to ~0.35 ml. The concentrated protein sample was loaded onto a Superose 6 Increase 10/300 GL size-exclusion column equilibrated with buffer that consists of 20 mM HEPES, pH 7.3, 250 mM NaCl, 4 mM DM, 20 mM imidazole, and 0.1 mg/ml POPS at 4 °C. The fractions containing the target protein were pooled and concentrated using the same concentrator. Protein concentration was measured using the 660-nm protein assay kit (Thermo Fisher Scientific).

Peptide synthesis and PORCN inhibitors

Substrate-mimicking peptides for WT or mutant Wnts with a point mutation, varying in lengths or the number of disulfide bonds, were purchased from CPC Scientific (Sunnyvale, CA) or synthesized in-house. All of the peptides used for this study had >95% purity. The peptides used for this study are listed in Fig. 3*A*. Full experimental details for the in-house synthesized peptides can be found in the supporting material. C59 (≥99% purity) and LGK974 (≥97% purity) inhibitors were purchased from Calbiochem.

Synthesis of Wnt peptides using solid-phase peptide synthesis—Linear peptides were synthesized by the Fmoc (*N*-(9-fluorenyl)methoxycarbonyl) solid-phase peptide synthesis method (43) using a 433A peptide synthesizer (Applied Biosystems). Rink amide resins (Sigma) were used as solid supports, and amino acids were coupled using HATU (Aapptec) and *N*,*N*′-diisopropylcarbodiimide (Thermo Fisher Scientific). For regioselective disulfide bond formation, cysteines with different protecting groups were used for the synthesis; the side chains of the first/fourth cysteines (in the primary sequence) and second/third cysteines were protected with an acetamidomethyl and trityl group, respectively. After the synthesis, synthesized peptides were released from the resins and deprotected in Reagent B (TFA/phenol/water/triisopropyl silane, 88:5:5:2) for 2–4 h at room temperature. The resins were removed by filtering through an empty gravity-flow column (Bio-Rad, Econo-Pac), and the filtrate was collected on ice-cold diethyl ether to precipitate peptides. Peptides were collected by centrifugation (2000 *g* x 5 min), and washed two times using diethyl ether. These crude linear peptides were dried under a vacuum desiccator overnight.

Formation of disulfide bonds—The formation of the disulfide bond formed by the second and third cysteines in the primary sequence was carried out in an oxidative condition using DMSO. Dry peptides were first dissolved in 20% acetonitrile containing 0.1% TFA to approximately 5 mg/ml and were added to the folding solution (0.1 M Tris-Cl, pH 7.8–8.3, 1 M guanidine hydrochloride, 1% DMSO, and 0.1 mM peptide) to initiate the formation of disulfide bond. After folding for 2–4 days at 4 °C, the pH of the solution was dropped to 2.5–3.5 to quench the folding reaction, and the solution was supplemented with 10% acetonitrile to prevent the nonspecific binding of peptides to plastic surfaces during the subsequent purification steps. The solution was filtered through a 0.22-μm disc membrane filter (Durapore, EMD Millipore), and the filtrate was loaded onto a C18 semi-prep column (10 × 250 mm) overnight using a 0.5–1.5-ml/min flow rate to remove salts. After extensive washing using H_2O containing 0.1% TFA, bound peptides were eluted using 70% acetonitrile containing 0.1% TFA. Peptide concentrations were estimated by using calculated molar extinction coefficients at 280 nm based on the sequence of peptides and by measuring the absorbance at 280 nm. The peptide solution was diluted to 0.1 mM using 20% acetonitrile containing 0.1% TFA for the next step.

The formation of the disulfide bond formed by the first and fourth cysteines was carried out by adding a 10–14-eq amount (in molar ratio) of iodine (0.1 M stock solution in methanol) to the peptide solution. The reaction was continued for 1 h at room temperature and quenched by adding ascorbic acid powder until the solution became colorless. For subsequent purification using ion-exchange chromatography, the solution was supplemented with sodium acetate (20 mM), and pH was adjusted to 3.0 using hydrochloric acid.

Purification of folded peptides using ion-exchange chromatography and reversed-phase HPLC

After completing the formation of disulfide bonds, the peptide solution was first loaded onto a cation-exchange chromatography column (HisTrap SP, 5 ml; GE Healthcare) using a 5-ml/min flow rate. The column was washed with buffer A (20 mM sodium citrate, pH 3.0, 10% acetonitrile) until a stable baseline was reached, and bound peptides were eluted by increasing buffer B (buffer A supplemented with 1 M NaCl) concentration from 0 to 100% for 40 min (200 column volumes), collecting 5-ml fractions. Peak containing peptide with the correct molecular weight was identified by analyzing each fraction using LC-MS. Finally, the peptide was purified by reversed-phased high-performance liquid chromatography (RP-HPLC) using a semi-prep C18 (10 × 250 mm; Waters BEH®) column, and the purity of purified peptide was confirmed by a run on an analytical C18 (4.6 × 250 mm; Waters BEH®) column before carrying out functional experiments. Water containing 0.1% TFA (solvent A) and acetonitrile containing 0.1% TFA (solvent B) were used for gradient elution in RP-HPLC purification. The gradient conditions for the RP-HPLC purification were as follows: increase of solvent B concentration from 20 to 35% for 15 min using 4.7 ml/min and 1 ml/min for semi-prep and analytical purification, respectively.

HPLC of acylated Wnt peptides

The reaction samples were prepared by adding 10 μl of the designated peptide (1 mM), 2 μl of palmitoleoyl-CoA (10 mM), and 10 μl of the purified hPORCN enzyme (25 μM) to 230 μl of a buffer containing 20 mM HEPES, pH 7.3, 150 mM NaCl, 4 mM DM, and 0.1 mg/ml POPS. The reaction mixture was incubated at 15 °C for 3 h and then was added to 250 μl of 80% acetonitrile solution containing 0.1% TFA. Prior to HPLC analysis, the precipitate was removed by centrifugation at 20,000 × *g* for 10 min. Then the reaction product was purified by reversed-phased HPLC using a preparative C4 (214TP, 10 × 250 mm; Grace®) column with the gradient conditions as follows: increase of solvent B concentration from 5 to 95% for 15 min using 5 ml/min. The solvent A and B are water containing 0.1% TFA and 80% acetonitrile solution containing 0.1% TFA, respectively. The target peaks were then analyzed by LC-MS.

LC-MS analysis of intact and acylated Wnt peptides

Wnt peptides were analyzed on a LC-MS system, which includes a 6320 TOF LC-MS mass spectrometer with a Dual AJS ESI source (Agilent), and a 1290 Infinity HPLC system with a 1290 autosampler (Agilent). Peptides were separated on a Poroshell 300SB-C3 column (1.0 × 75 mm, 5 μm; Agilent) with a 6-min linear gradient of 20–80% mobile phase B at a flow rate of 300 μl/min. Mobile phase A is composed of 97.9% water, 2% acetonitrile, and 0.1% formic acid. Mobile phase B contains 98% acetonitrile, 1.9% water, and 0.1% formic acid. The purity of all reagents used in the analysis was HPLC grade. The Vcap and nozzle voltages were 4500 and 1000 V, respectively. The MS data acquisition was performed in positive mode with a mass range of m/z 400–3200. LC-MS data were analyzed using Agilent MassHunter Qualitative Analysis B.07.00 software.

Coupled-enzyme assay

To measure rates of hPORCN-catalyzed palmitoleoylation, we adopted and modified a fluorescence-based coupled-enzyme assay described previously (33). The kinetic assays were carried out in 384-well low-volume plates (Thermo Fisher Scientific) at 25 °C. Plates were read in a Tecan M1000Pro instrument. Prior to the start of the assay, 10 μl of reaction solution A (0.25 mM oxidized NADH (NAD^+), 0.2 mM thiamine pyrophosphate, 2 mM 2-oxoglutarate, and fatty acyl-CoA substrate in a buffer containing 20 mM HEPES, pH 7.3, 150 mM NaCl, 4 mM DM, and 0.1 mg/ml POPS) and 10 μl of reaction solution B (αKDH and peptide substrate in the same buffer) were mixed. For the pH dependence assay, 20 mM HEPES, pH 7.3, in the buffer was replaced with the same concentration of MES for pH 6.0–6.5, HEPES for pH 7.0–7.5, and Tris-HCl for pH 8.0–9.5, respectively. The αKDH was prepared in-house as described previously (44). To determine the optimal concentration of αKDH required for the assay, αKDH was titrated until the slope of the reaction progress curve become constant. The purified hPORCN enzyme was added into the assay mixture to initiate the reaction (2 μl into 20 μl). To analyze the reaction rates, NADH production was monitored with 340-nm excitation and 465-nm emission for 15 min. The linear part of reaction progression curve was used to determine initial velocities derived from the hPORCN-catalyzed reactions. The background signals resulting from the spontaneous hydrolysis of fatty acyl-CoAs were subtracted from the initial velocities. To determine apparent K_m values in the two-substrate system, the rates were measured by varying the concentrations of one substrate at saturating concentration of the other substrate. The data were fitted to the Michaelis–Menten model using the nonlinear least square function in GraphPad Prism version 6, obtaining the kinetic parameters (Fig. S4). All enzymatic assays were performed in triplicate.

To determine the IC_{50} of C59, the compound was serially diluted (1 nM to 100 μM) in 10 μl of reaction solution A holding a 2% DMSO concentration. 2 μl of purified hPORCN enzyme was added into the solution, followed by incubation at room temperature for 5 min. Then the reaction was initiated by adding 10 μl of reaction solution B, to give final concentrations of 200 nM hPORCN, 50 μM hWnt1p peptide, and 50 μM palmitoleoyl-CoA. The IC_{50} of C59 was calculated based on the inhibition of NADH fluorescence signaling. The data were collected and analyzed as described above.

For the hDHCH20 fatty acyl-CoA selectivity experiments, the assay was done as published (31) with minor changes. Reaction buffer was changed from MES to HEPES at pH 7.0, and the assay was done in a 384-well plate instead of a 96-well plate with a total reaction volume of 40 μl.

Isothermal titration calorimetry

hPORCN protein sample was purified in the same manner as described above, except that the final buffer for size-exclusion chromatography consisted of 25 mM HEPES, pH 7.5, 300 mM NaCl, 4 mM DM, and 0.1 mg/ml POPS. The same buffer with 1% DMSO was used to prepare LGK974 inhibitor titrant. Prior to the experiment, 1% DMSO was added to the protein sample for

buffer matching. Data were collected during 15 3-μl injections of 250 μM inhibitor into 15–25 μM of hPORCN at 18 °C with stirring at 480 rpm and 180-s injection spacing, using a MicroCal i200 microcalorimeter (Malvern Instruments). The heat exchanged during each injection was integrated using NITPIC version 1.2.0 (45) and fit to nonlinear regression analysis as a single-site binding using SEDPHAT version 12.1b, obtaining thermodynamic parameters. GUSSI version 1.1.0 (45) was used to plot the processed data.

Author contributions—C.-J. L., M. R., C. B., and Y. L. formal analysis; C.-J. L., M. R., C. B., and Y. L. investigation; C.-J. L., M. R., C. B., and A. B. methodology; C.-J. L. and A. B. writing-original draft; A. B. conceptualization; A. B. resources; A. B. supervision; A. B. funding acquisition; A. B. project administration.

Acknowledgments—We thank Chad Williamson (National Institutes of Health) for the ER marker and for help with confocal imaging and Gisela Storz (National Institutes of Health) and Kenton Swartz (National Institutes of Health) for comments on the manuscript.

References

1. Clevers, H., and Nusse, R. (2012) Wnt/β-catenin signaling and disease. *Cell* **149,** 1192–1205 CrossRef Medline
2. Lim, X., Tan, S. H., Koh, W. L., Chau, R. M., Yan, K. S., Kuo, C. J., van Amerongen, R., Klein, A. M., and Nusse, R. (2013) Interfollicular epidermal stem cells self-renew via autocrine Wnt signaling. *Science* **342,** 1226–1230 CrossRef Medline
3. Wang, J., Sinha, T., and Wynshaw-Boris, A. (2012) Wnt signaling in mammalian development: lessons from mouse genetics. *Cold Spring Harb. Perspect. Biol.* **4,** a007963 CrossRef Medline
4. Gao, X., and Hannoush, R. N. (2014) Single-cell imaging of Wnt palmitoylation by the acyltransferase porcupine. *Nat. Chem. Biol.* **10,** 61–68 CrossRef Medline
5. Janda, C. Y., Waghray, D., Levin, A. M., Thomas, C., and Garcia, K. C. (2012) Structural basis of Wnt recognition by Frizzled. *Science* **337,** 59–64 CrossRef Medline
6. Rios-Esteves, J., and Resh, M. D. (2013) Stearoyl CoA desaturase is required to produce active, lipid-modified Wnt proteins. *Cell Rep.* **4,** 1072–1081 CrossRef Medline
7. Takada, R., Satomi, Y., Kurata, T., Ueno, N., Norioka, S., Kondoh, H., Takao, T., and Takada, S. (2006) Monounsaturated fatty acid modification of Wnt protein: its role in Wnt secretion. *Dev. Cell* **11,** 791–801 CrossRef Medline
8. Zhai, L., Chaturvedi, D., and Cumberledge, S. (2004) *Drosophila* wnt-1 undergoes a hydrophobic modification and is targeted to lipid rafts, a process that requires Porcupine. *J. Biol. Chem.* **279,** 33220–33227 CrossRef Medline
9. Willert, K., Brown, J. D., Danenberg, E., Duncan, A. W., Weissman, I. L., Reya, T., Yates, J. R., 3rd, Nusse, R. (2003) Wnt proteins are lipid-modified and can act as stem cell growth factors. *Nature* **423,** 448–452 CrossRef Medline
10. Hofmann, K. (2000) A superfamily of membrane-bound *O*-acyltransferases with implications for wnt signaling. *Trends Biochem. Sci.* **25,** 111–112 CrossRef Medline
11. Resh, M. D. (2013) Covalent lipid modifications of proteins. *Curr. Biol.* **23,** R431–R435 CrossRef Medline
12. Lim, X., and Nusse, R. (2013) Wnt signaling in skin development, homeostasis, and disease. *Cold Spring Harb. Perspect. Biol.* **5,** a008029 Medline CrossRef
13. Proffitt, K. D., Madan, B., Ke, Z., Pendharkar, V., Ding, L., Lee, M. A., Hannoush, R. N., and Virshup, D. M. (2013) Pharmacological inhibition of the Wnt acyltransferase PORCN prevents growth of WNT-driven mammary cancer. *Cancer Res.* **73,** 502–507 CrossRef Medline
14. Covey, T. M., Kaur, S., Tan Ong, T., Proffitt, K. D., Wu, Y., Tan, P., and Virshup, D. M. (2012) PORCN moonlights in a Wnt-independent pathway that regulates cancer cell proliferation. *PLoS One* **7,** e34532 CrossRef Medline
15. Willert, K., and Nusse, R. (2012) Wnt proteins. *Cold Spring Harb. Perspect. Biol.* **4,** a007864 Medline
16. Cheng, Y., Phoon, Y. P., Jin, X., Chong, S. Y., Ip, J. C., Wong, B. W., and Lung, M. L. (2015) Wnt-C59 arrests stemness and suppresses growth of nasopharyngeal carcinoma in mice by inhibiting the Wnt pathway in the tumor microenvironment. *Oncotarget* **6,** 14428–14439 Medline
17. Liu, J., Pan, S., Hsieh, M. H., Ng, N., Sun, F., Wang, T., Kasibhatla, S., Schuller, A. G., Li, A. G., Cheng, D., Li, J., Tompkins, C., Pferdekamper, A., Steffy, A., Cheng, J., *et al.* (2013) Targeting Wnt-driven cancer through the inhibition of Porcupine by LGK974. *Proc. Natl. Acad. Sci. U.S.A.* **110,** 20224–20229 CrossRef Medline
18. Madan, B., Ke, Z., Harmston, N., Ho, S. Y., Frois, A. O., Alam, J., Jeyaraj, D. A., Pendharkar, V., Ghosh, K., Virshup, I. H., Manoharan, V., Ong, E. H., Sangthongpitag, K., Hill, J., Petretto, E., *et al.* (2016) Wnt addiction of genetically defined cancers reversed by PORCN inhibition. *Oncogene* **35,** 2197–2207 CrossRef Medline
19. Wang, X., Moon, J., Dodge, M. E., Pan, X., Zhang, L., Hanson, J. M., Tuladhar, R., Ma, Z., Shi, H., Williams, N. S., Amatruda, J. F., Carroll, T. J., Lum, L., and Chen, C. (2013) The development of highly potent inhibitors for porcupine. *J. Med. Chem.* **56,** 2700–2704 CrossRef Medline
20. Dodge, M. E., Moon, J., Tuladhar, R., Lu, J., Jacob, L. S., Zhang, L. S., Shi, H., Wang, X., Moro, E., Mongera, A., Argenton, F., Karner, C. M., Carroll, T. J., Chen, C., Amatruda, J. F., and Lum, L. (2012) Diverse chemical scaffolds support direct inhibition of the membrane-bound *O*-acyltransferase porcupine. *J. Biol. Chem.* **287,** 23246–23254 CrossRef Medline
21. Asciolla, J. J., Miele, M. M., Hendrickson, R. C., and Resh, M. D. (2017) An *in vitro* fatty acylation assay reveals a mechanism for Wnt recognition by the acyltransferase Porcupine. *J. Biol. Chem.* **292,** 13507–13513 CrossRef Medline
22. Proffitt, K. D., and Virshup, D. M. (2012) Precise regulation of Porcupine activity is required for physiological Wnt signaling. *J. Biol. Chem.* **287,** 34167–34178 CrossRef Medline
23. Nile, A. H., and Hannoush, R. N. (2016) Fatty acylation of Wnt proteins. *Nat. Chem. Biol.* **12,** 60–69 CrossRef Medline
24. Rios-Esteves, J., Haugen, B., and Resh, M. D. (2014) Identification of key residues and regions important for porcupine-mediated Wnt acylation. *J. Biol. Chem.* **289,** 17009–17019 CrossRef Medline
25. Lorenz, H., Hailey, D. W., Wunder, C., and Lippincott-Schwartz, J. (2006) The fluorescence protease protection (FPP) assay to determine protein localization and membrane topology. *Nat. Protoc.* **1,** 276–279 CrossRef Medline
26. Matevossian, A., and Resh, M. D. (2015) Membrane topology of Hedgehog acyltransferase. *J. Biol. Chem.* **290,** 2235–2243 CrossRef Medline
27. Konitsiotis, A. D., Jovanović, B., Ciepla, P., Spitaler, M., Lanyon-Hogg, T., Tate, E. W., and Magee, A. I. (2015) Topological analysis of Hedgehog acyltransferase, a multipalmitoylated transmembrane protein. *J. Biol. Chem.* **290,** 3293–3307 CrossRef Medline
28. Taylor, M. S., Ruch, T. R., Hsiao, P. Y., Hwang, Y., Zhang, P., Dai, L., Huang, C. R., Berndsen, C. E., Kim, M. S., Pandey, A., Wolberger, C., Marmorstein, R., Machamer, C., Boeke, J. D., and Cole, P. A. (2013) Architectural organization of the metabolic regulatory enzyme ghrelin O-acyltransferase. *J. Biol. Chem.* **288,** 32211–32228 CrossRef Medline
29. Dhamdhere, G. R., Fang, M. Y., Jiang, J., Lee, K., Cheng, D., Olveda, R. C., Liu, B., Mulligan, K. A., Carlson, J. C., Ransom, R. C., Weis, W. I., and Helms, J. A. (2014) Drugging a stem cell compartment using Wnt3a protein as a therapeutic. *PLoS One* **9,** e83650 CrossRef Medline
30. Galli, L. M., Barnes, T. L., Secrest, S. S., Kadowaki, T., and Burrus, L. W. (2007) Porcupine-mediated lipid-modification regulates the activity and distribution of Wnt proteins in the chick neural tube. *Development* **134,** 3339–3348 CrossRef Medline
31. Rana, M. S., Kumar, P., Lee, C. J., Verardi, R., Rajashankar, K. R., and Banerjee, A. (2018) Fatty acyl recognition and transfer by an integral membrane *S*-acyltransferase. *Science* **359,** eaao6326 CrossRef Medline
32. Mitchell, D. A., Mitchell, G., Ling, Y., Budde, C., and Deschenes, R. J. (2010) Mutational analysis of *Saccharomyces cerevisiae* Erf2 reveals a two-

step reaction mechanism for protein palmitoylation by DHHC enzymes. *J. Biol. Chem.* **285,** 38104–38114 CrossRef Medline
33. Hamel, L. D., Deschenes, R. J., and Mitchell, D. A. (2014) A fluorescence-based assay to monitor autopalmitoylation of zDHHC proteins applicable to high-throughput screening. *Anal. Biochem.* **460,** 1–8 CrossRef Medline
34. Bai, Y., McCoy, J. G., Levin, E. J., Sobrado, P., Rajashankar, K. R., Fox, B. G., and Zhou, M. (2015) X-ray structure of a mammalian stearoyl-CoA desaturase. *Nature* **524,** 252–256 CrossRef Medline
35. Wang, H., Klein, M. G., Zou, H., Lane, W., Snell, G., Levin, I., Li, K., and Sang, B. C. (2015) Crystal structure of human stearoyl-coenzyme A desaturase in complex with substrate. *Nat. Struct. Mol. Biol.* **22,** 581–585 CrossRef Medline
36. Kakugawa, S., Langton, P. F., Zebisch, M., Howell, S., Chang, T. H., Liu, Y., Feizi, T., Bineva, G., O'Reilly, N., Snijders, A. P., Jones, E. Y., and Vincent, J. P. (2015) Notum deacylates Wnt proteins to suppress signalling activity. *Nature* **519,** 187–192 CrossRef Medline
37. Jennings, B. C., and Linder, M. E. (2012) DHHC protein *S*-acyltransferases use similar ping-pong kinetic mechanisms but display different acyl-CoA specificities. *J. Biol. Chem.* **287,** 7236–7245 CrossRef Medline
38. Ulrich, A., Andersen, K. R., and Schwartz, T. U. (2012) Exponential megapriming PCR (EMP) cloning–seamless DNA insertion into any target plasmid without sequence constraints. *PLoS One* **7,** e53360 CrossRef Medline
39. Gibson, D. G., Young, L., Chuang, R. Y., Venter, J. C., Hutchison, C. A., 3rd, Smith, H. O. (2009) Enzymatic assembly of DNA molecules up to several hundred kilobases. *Nat. Methods* **6,** 343–345 CrossRef Medline
40. Snapp, E. L., Sharma, A., Lippincott-Schwartz, J., and Hegde, R. S. (2006) Monitoring chaperone engagement of substrates in the endoplasmic reticulum of live cells. *Proc. Natl. Acad. Sci. U.S.A.* **103,** 6536–6541 CrossRef Medline
41. Schindelin, J., Arganda-Carreras, I., Frise, E., Kaynig, V., Longair, M., Pietzsch, T., Preibisch, S., Rueden, C., Saalfeld, S., Schmid, B., Tinevez, J. Y., White, D. J., Hartenstein, V., Eliceiri, K., Tomancak, P., and Cardona, A. (2012) Fiji: an open-source platform for biological-image analysis. *Nat. Methods* **9,** 676–682 CrossRef Medline
42. Kawate, T., and Gouaux, E. (2006) Fluorescence-detection size-exclusion chromatography for precrystallization screening of integral membrane proteins. *Structure* **14,** 673–681 CrossRef Medline
43. Chan, W. C., and White, P. D. (2000) *Fmoc Solid Phase Peptide Synthesis: A Practical Approach*, pp. 41–76, Oxford University Press, New York
44. Stanley, C. J., and Perham, R. N. (1980) Purification of 2-oxo acid dehydrogenase multienzyme complexes from ox heart by a new method. *Biochem. J.* **191,** 147–154 CrossRef Medline
45. Brautigam, C. A., Zhao, H., Vargas, C., Keller, S., and Schuck, P. (2016) Integration and global analysis of isothermal titration calorimetry data for studying macromolecular interactions. *Nat. Protoc.* **11,** 882–894 CrossRef Medline